The International Joint Conferences

Surfaces, Coatings and Interfaces
SurfCoat Korea 2019
&
Graphene Korea 2019

Mar 27 to 29, 2019, Incheon/Seoul - Korea

Conference Proceedings

DOI: https://doi.org/10.26799/cp-surfcoat-graphene-korea-2019

Corona Discharge Mitigation for HVAC Transmission Lines by Surface Modification

Nurkhat Zhakiyev[1], Kurbangali Tynyshtykbayev[1], Jim Norem[2], Zinetula (Zeke) Insepov[1,3,4*]

[1] Nazarbayev University
53 Kabanbay Batyr Ave, Nur-Sultan, Kazakhstan, zinsepov@nu.edu.kz
[2] Nanosynergy Corp. Downers Grove, IL USA
[3] National Research Nuclear University MEPhI, 31 Kashira Highway, Moscow, Russia
[4, †*] Purdue University, 500 Central Drive, West Lafayette, IN USA, zinsepov@purdue.edu

Abstract

Mitigation of corona discharge is fundamental problem that was formulated by Lord Kelvin in 1911 but has not yet received a proper technical solution. On HVAC transmission lines up to 30% of the total electric power losses accounted for corona discharge (CD). A peak of losses occurs during adverse (wet) weather conditions, such as rain and snow. Coating on the surface of aluminium wire using microarc oxidation (MAO), also known as electrolytic plasma oxidation (EPO) was implemented to reduce losses due to CD. Samples covered by the surface with porous high-temperature α-Al_2O_3 aluminium oxide, silicon oxide SiO_2, silicon carbide SiC reinforced with graphene oxide and carbon nanotubes. Industrial high-voltage testing shows that the significant reduction of the power loss due to corona of 30-50% has been measured in the present work where wires were coated with strong, adhesive, and super-hydrophilic layer. The corona ignition threshold voltage increased up to 40% in the rain conditions, and up to 15% for dry conditions. Simulations using finite element method (FEM) have shown a significant dependence of a local electric field enhancement factor on the surface wettability (hydrophilicity). Highly porous and hygroscopic properties of newly engineered surfaces allow to control contact angle of a water droplet on the wire and reduce the field enhancement factor in comparison with a uncoated surface via the effect of dielectric shielding.

Keywords: Anti-corona coating, microarc oxidation, HVAC, corona-discharge, Electric field mitigation.

1. Introduction

A significant amount of the power grid based on the overhead high voltage alternating current (HVAC) transmission lines due to large transmission capacity and economic feasibility. However, up to 30% of electric power losses are associated with corona discharge (CD), especially, under adverse weather conditions, such as rain and snow [1-3]. Thus, it is urgently need to find a new way to reduce the corona losses, especially under rain conditions. The research on the anti-corona coating is relatively little, main aims of the anti-corona coating proposals is changing hydrophobicity/hydrophilicity of surface, such as RTV (Room Temperature Vulcanisation) or fiber textile coatings [4, 5]. One of the coating methods with relatively low cost for changing hydrophilicity is microarc oxidation (MAO). Compact ceramic coatings using MAO is an attractive topic in the field of metal protection with the good characteristics including their remarkable thickness, high microhardness, high porous, insulation resistance, and good adhesion with substrates [6]. The influence of rainfall intensity on AC corona discharge with the radio interference level investigated in [7], plasma-water interaction phenomena were investigated and experiments supported by computer modelling in [8, 9]. In this paper, the surface MAO coating electrolyte solution improved with particle additions for corona-discharge mitigation purposes and tested on HVAC industrial size climate chamber. The characterisation of MAO coating also provided.

2. Experimental
2.1. MAO Coating

In this work, the samples of non-insulated (bare) industrial aluminium wires of AC300/39[10] for 500 kV HVAC air transmission lines were used for the study. Here shown results for two types of electrolytes which were used for MAO. For sample A4 used electrolyte solution (NaOH (3 g/l), $Na_4P_2O_7$ (4 g/l), Na_2SiO_3 (15 g/l), $C_3H_8O_3$ (10 ml/l), Al_2O_3 (50 mg/l) with additives of a suspension of exhaust gas (2 mg GO/ml H_2O) manufactured by Sigma Aldrich, USA. For sample A5 in the electrolyte solution the GO suspension

replaced by CNT suspension (50 g 0.01% by weight of CNT per 100 ml of $C_3H_8O_3$) manufactured by TUBALL, Novosibirsk, Russia. Depositing thin films on wire samples with a length of 1500 mm by MAO was carried out using a pulsed DC of up to 3 A passing through an electrolysis equipment consisting of a negative Al- electrode (cathode), an electrolyte, and a positive electrode the Al- wire sample (anode). A stepwise voltage in a range from 160V to 320V with steps of 20V was applied for each wire sample for 4 hours. By MAO thin film coatings of 15 μm in thickness, with different porosity and wettability, were deposited on the surfaces of aluminium wire samples (See section 3).

2.2. Characterisation

Morphology and elemental composition of the deposited thin film coatings were visualized with a scanning electron Crossbeam 540 with an energy dispersive analyser and an optical LSM 780, Carl Zeiss microscopes, and characterized by an XRD method (Smartlab, Rigaku, XRF Panalytical). Separate measurements were carried out using a scanning electron microscope TESCAN LYRA3 GMH, St. Petersburg. The EDS spectra show that the main elements (with more than 10% by weight) in the deposited coatings of samples A4 and A5 are Al, Si and O, (See Table 1). Sample A0 contain the main element Al, 99.42%.

Table 1. Basic elements of the composition of coatings

Sample	EDS spectra			XRF analyze		
	Al, %	O, %	Si, %	Al_2O_3, %	SiO_2, %	P_2O_5, %
A0	99.42	-	-	-	-	-
A4	20.35	41.77	19.19	36.9%	35.4%	9.0%
A5	12.34	49.94	26.53	37.1%	32.0%	21.5%

The results of X-ray fluorescence XRF analysis showed that the coatings consist mainly of aluminium oxides Al_2O_3 and silicon SiO_2: - sample A4 contains 36.9% Al_2O_3, 35.4% SiO_2, 9.0% P_2O_5; sample A5 contains 37.1% Al_2O_3, 32.0% SiO_2, 21.5% P_2O_5 (See Table 1). Carbon and carbon compounds, which were one of the main components of the coating composition, were not recorded by the XRF and EDS characterization methods. However, X-ray diffraction XRD spectra showed that the coating composition contained carbon compounds with silicon and aluminium, silicon carbide SiC and silumin AlSi. A silumin (AlSi) was obtained in the deposited coatings for all test samples which can be explained due to the presence of the sodium salt Na_2SiO_3 (sodium metasilicate) in the main electrolyte. Our analysis of EDS-, XRF- and XRD-spectra shows that the main compounds that makes up the coatings are Al_2O_3, SiO_2, AlSi and SiC. The chemical analysis of the elemental coating content was based on the EDS microanalysis data. The results that were based on the stoichiometry of the main compounds Al_2O_3, SiO_2, AlSi and SiC show the same carbon content in all coatings of about 31.35%, with slight variations.

Table 2. Wettability and contact angle of samples

	A0	A4	A5
Wettability, amount of water before and after, mg.	5363.1/5364.1 (Δ1.1)	5382.7/5396.2 (Δ13.5)	5675.7/5684.2 (Δ8.5)
α – contact angle, deg.	α≈46^0-56^0	α≈24^0	α<24^0

The highest porosity and wettability were provided by depositing coatings with additives of nanoparticles of graphene oxide (sample A4) and carbon nanotubes (sample A5). The wettability of the deposited coatings was measured on the control wires, with a diameter of 4 mm and a length of 180 mm. The weight of the samples A4 and A5 after wetting with water has increased by 13.5 mg and 8.5 mg respectively, as compared to the weight increase of the original sample A0 (1.1 mg increase). That is, the high wettability (Table 2) of the coatings of samples A4 and A5 was related to the high porosity of the coating surface (Fig.1).
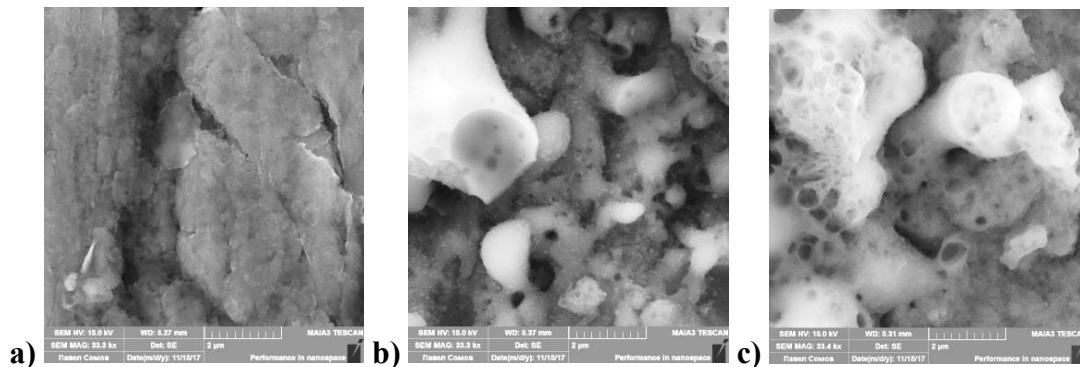
Fig. 1. EM images of wire surface samples: a) A0, b) A4, c) A5[10]

2.3. HVAC industrial test

HVAC with industrial frequency (50 Hz) were carried out on a wire-plane electrode system reproduced with scale to 1:2.38 by voltage which corresponds to the 500 kV level with the same electric field in the real conditions. A series of experiments with the step of increasing and decreasing the voltage to 20 kV were carried out both for rain (50-170-50 kV) and dry climate conditions (100-200-100 kV). The voltage of the onset of corona discharges was determined by the optical method using the electron-optical flaw detector (EOFD) "Filin-6", the discharge lightning including the invisible ultraviolet spectral region was recorded using a photomultiplier tube "PMT-119", which are synchronized with a digital oscilloscope. The rainfall was simulated using a nozzle sprayer located above the wire at a height of 112 cm which covered the entire length of the sample. In each series of experiments, a preliminary exposure of the wire in the rain for at least 5 minutes was provided. The intensity of rain (~0.9 mm/min) fixed for all samples. The power loss for the corona was determined by numerical integration of the volt-charging characteristics.

3. Computer modelling of dielectric shielding

Electric field enhancement factor (β-factor) on the micro-size tip on the electrode can provide a good condition for arising corona discharge [11]. Finite Element Method (FEM) used for modelling dry and wetted wires with 10 um tip on surface according to the contact angels from Tabel 2. In a dry conditions local electric field around a micro-size tip increased up to $\beta=5.4$. This β factor can be reduced by dielectric shielding effect if water layer covered the surface with low contact angle. In the Fig.3a. shown calculated β-factor for two samples of wires.
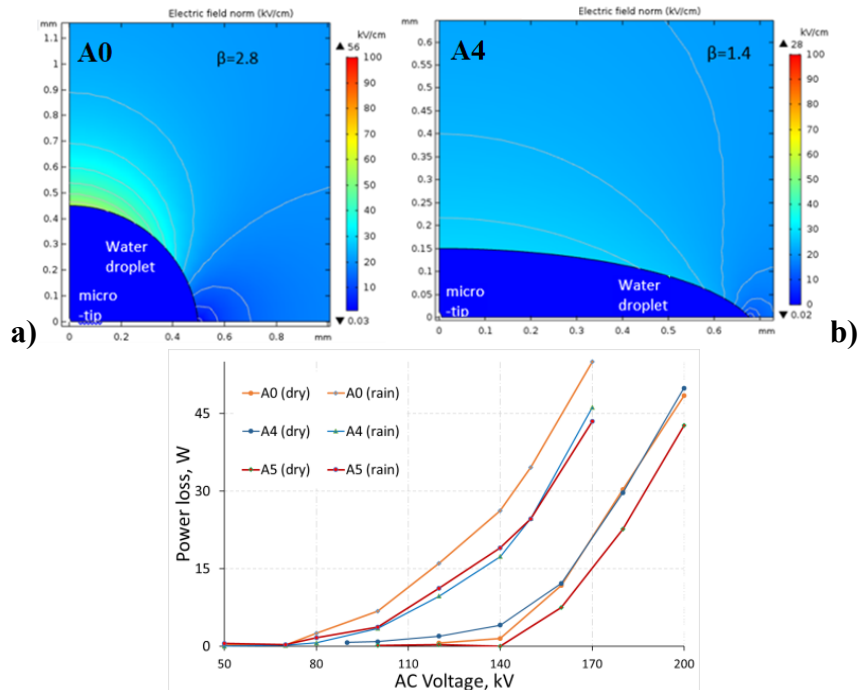
Fig.3. a) β-factors for droplets on samples A0($\alpha \approx 46^0$) and A4($\alpha \approx 24^0$); b) HVAC test results

4. Results and discussions

Our results confirm the well-known facts that CD in the rain occur at a significantly lower voltage than in the dry state [2]. For example, the CD triggering voltage on the uncoated reference wire in a dry climate was measured to be 144 kV. The same wire coated with a thin film showed that corona discharge is triggered at $V_{CD} = 83$ kV for a rain climate. Compared with the triggering CD voltage in the dry state, the voltage of the beginning of the CD in the rain decreased by a factor of 1.3-1.4. And the power losses for CD increased by more than an order of magnitude at a scaled voltage of 120 kV corresponding to an average operating voltage of 290 kV, the power of corona losses on coated wires in rain conditions was reduced by approximately 40% compared to an uncoated wire. The power losses on the corona discharge in rain conditions are much lower for the A4 and A5[10] coated samples than for the reference sample A0. The results of high-voltage breakdown tests of samples in the dry climate conditions are also show reduced losses (Fig. 3b). From the results of high-voltage breakdown tests of samples in dry climate conditions the highest anti-corona resistance was observed on the sample A5. The increase in the CD triggering voltage for the sample A5 reached up to 15%, as compared with the triggering voltage of the original sample A0, and the power losses for corona was much lower than that by approximately 30-50% (Fig. 3b).

5. Conclusion

A new method of a high-corona discharge resistance coating on aluminium wires has been developed and investigated. High anti-corona resistance of wire samples was achieved by depositing MAO coatings based on the high-temperature α-Al_2O_3 alloys, SiO_2, AlSi and SiC, reinforced with particle additions GO and CNT. Coating has high porosity, hydrophilicity, and hygroscopicity properties that reduces the number of local CD foci (up to 40% in rain).

Electrostatic model based on FEM has shown that the field enhancement factor can be decreased due to dielectric shielding by water. During the rainfall, droplet formation geometry plays an important role in formation of field enhanced spots.

Significant decrease of the power loss due to corona of 30-40% has been measured. At the same time, the voltage of the corona ignition increased for rain by 40% and for dry by 15%. Thus, a higher anti-corona resistance of aluminium wire samples in rain conditions was achieved using a higher hydrophilicity of the coatings. An increase of water wettability of the surface would reduce the electrical field enhancement factor and therefore, reduce the power losses in measured samples.

References

1. W. F. Long and J. P. Stovall "Comparison of costs and benefits for DC and AC transmission," *C.I.G.R.E. AC/DC Transmission Interactions and Comparison Symp.,* 1987
2. U. Straumann, "Mechanism of the tonal emission from ac high voltage overhead transmission lines," *Journal of Physics D: Applied Physics*, (2011). 44(7), 075501.
3. L. Chen, X. Bian, L. Wang, Z. Guan "Effect of rain drops on corona discharge in alternating current transmission lines with a corona cage" *Japanese Journal of Applied Physics*, 2012, 51(9S2), 09MG02.
4. Z. Xu, R. Li "Research on the Anti-corona Coating of the Power Transmission Line Conductor," *Energy and Power Engineering,* 2013, 5, 148-150.
5. G. Riquel and A. Gayrard, "High voltage overhead electrical conductor`s corona effect reducing device, has conductor sheath including fiber textile material for absorbing water coming at its contact and band rolled around high voltage conductor," *Patent FR2874283A1,* August 12, 2004
6. X. Lu, M. Mohedano, C. Blawert, E. Matykina, R. Arrabal, K. Kainer, M. Zheludkevich "Plasma electrolytic oxidation coatings with particle additions–a review," *Surface and Coatings Technology*, 2016, 307, 1165-1182.
7. P. Xu, B. Zhang, Z. Wang, S. Chen, J. He. (2017). Dynamic characteristics of corona discharge generated under rainfall condition on AC charged conductors. *Journal of Physics D: Applied Physics*, 50(50), 505206.
8. P. Vanraes, A. Bogaerts "Plasma physics of liquids-A focused review," *Applied Physics Reviews*, 2018, 5(3), 031103.
9. P. Vanraes, A. Nikiforov, A. Bogaerts, Ch. Leys. "Study of an AC dielectric barrier single micro-discharge filament over a water film," *Nature. Scientific Reports* | (2018) 8:10919 | DOI:10.1038/s41598-018-29189-w
10. K. B. Tynyshtykbaev, G. Z. Imanbaev, A. M. Ainabaev, et al. Reducing Power Losses in Corona Discharge under Rainfall Conditions. *Tech. Phys. Lett.* (2018) 44: 545. https://doi.org/10.1134/S1063785018060287
11. Z. Insepov & J. Norem "Can surface cracks and unipolar arcs explain breakdown and gradient limits?" *Journal of Vacuum Science & Technology A: Vacuum, Surfaces, and Films*, 2013, 31(1), 011302.

Influence of processing conditions on deposit layer formation by barrel nitriding treatment on aluminum alloy

Koichiro NAMBU[1], Kazuki Sayo[1] and Masahiro Okumiya[1]
[1]Toyota Technological Institute/Japan

2-12-1 Hisakata, Tenpaku-ku, Nagoya, Aichi, Japan, knambu @toyota-ti.ac.jp

Abstract

In recent years, demand for aluminum alloys has increased in transportation equipment such as automobiles. However, since the strength is lower than that of steel, high strength by surface treatment is required. Nitriding is one of surface treatments. The nitriding treatment can improve hardness and frictional wear characteristics by forming aluminum nitride on the surface. For the formation of AlN, a reduction nitriding method, an ion nitriding method, or the like can be mentioned. Since the former is a process above the melting point, it can not be processed, and the latter has a problem that the processing time is long. In this study, the barrel nitriding method was focused at a temperature lower than the melting point of Al and short process time. However, in the barrel nitriding process, there is a problem that a deposition layer is formed as AlN is formed and the surface shape is deteriorated. In this study it has been investigated the effects of processing conditions on the formation of the deposited layer

Keywords: Surface modification, Barrel nitriding, Aluminum Nitrid, diffusion.

1. Introduction

In recent years, resource saving and energy saving are required from the viewpoint of global environmental problems. Due to such social conditions, development of materials that are lightweight and high in strength is proceeding in transportation equipment such as automobiles. One of the light metal materials is an aluminum alloy. Aluminum alloys used in automobiles are only about 10% of constituent materials. Although the aluminum alloy is lightweight but its strength is lower than that of steel, it is used only for exterior and relatively low load parts. For resource saving and energy saving, it is necessary to add more value to aluminum and increase the number of parts applied to transportation equipment. In order to increase the number of applications to be applied, "improvement of hardness" and "improvement of wear resistance" can be cited as one of the necessary characteristics[1]-[5].

Various sliding parts exist in automobiles, but at present most of them do not use aluminum alloys. It is said that a hardness of 500 HV or more is necessary for use at such a sliding portion. At the present time, alumite treatment is mentioned as a representative of surface modification treatment on aluminum alloy. However, the hardness obtained by alumite treatment is low, on the order of 300 to 400 HV, and a different treatment is required. The aluminum alloy has a problem that the surface modification treatment is difficult due to the oxide film present on the surface and the low melting point. In order to overcome this problem, an ion nitridation method using pre-sputtering has been developed. However, the problem is that the processing time is extremely long.

In this research, the barrel nitriding treatment method attracted attention as a method to solve the problem of the conventional method. The barrel nitriding process is conceived from a barrel polishing apparatus used as a polishing machine, and is a method of performing a nitriding treatment while rotating a nitriding furnace like a polishing machine. In our previous research we have successfully nitrided aluminum particles. However, under the present conditions, there is a problem that a deposited layer is formed on the surface and the surface shape deteriorates.In this paper, a barrel nitriding treatment was performed on an aluminum sheet, and the relationship between processing conditions and sedimentary layer was studied.

2. Barrel Nitriding Process

A schematic view of a barrel nitriding apparatus is shown in Fig. 1. As shown in the figure, the material to be treated, the abrasive and the activator were installed in the chamber. At the same time, nitriding treatment is performed by introducing nitrogen into the chamber. By rotating the chamber, the oxide on the aluminum

surface can be physically removed by the abrasive. Since a small amount of oxygen remains in the chamber, a new oxide is formed immediately after removing the oxide. Therefore, by using Al - Mg alloy containing Mg which has higher reactivity with oxygen than aluminum as the active material, generation of oxides is prevented.
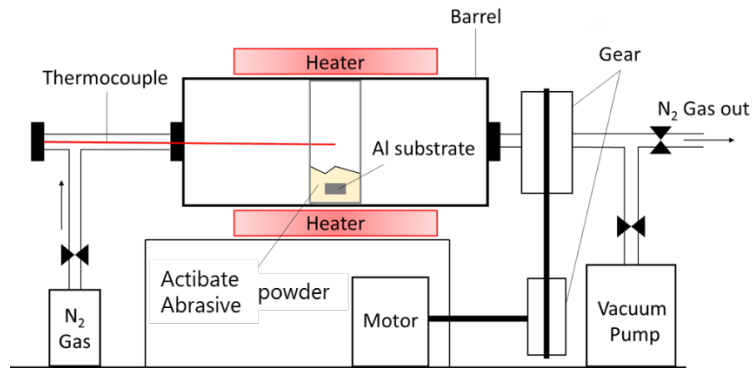

Fig. 1 Schematic of barrel nitriding

3. Specimen, heat pattern and analytical instrument

The test piece used was a round bar of aluminum alloy 5052 having a thickness of 3 mm and a diameter of 20 mm. Table 1 shows the chemical composition. Alumina powder was used as an abrasive. Alumina powder is a powder used in general barrel processing, and is selected as an abrasive because it is inexpensive and easily available and suitable for industrialization. Also, Al-10 wt. % Mg alloy powder was used as an activator. Table 2 shows the conditions selected to achieve "deposition layer suppression, AlN film thickness 100 μm, AlN layer Vickers hardness 500 HV or more". After processing under three conditions, hardness measurement and observation by SEM were performed.

Table1 Chemical compositions of 5052 alloy

	Si	Fe	Cu	Mg	Zn	Cr	Ti	Al
A5052	~0.25	~0.40	~0.1	2.2～2.8	~0.1	0.15～0.35	-	bal.

Table 2 Barrel nitriding conditions

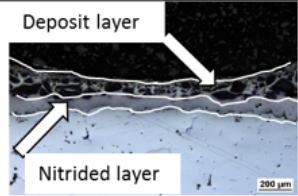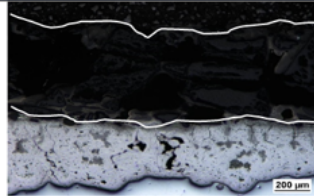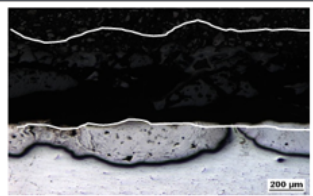|	Barrel nitriding conditions		
	1	2	3
Specimens	A5052		
Abrasive powder	Alumina (d:510-710μm), 300g		
Activator	Al-Mg Powder, 5g		
N_2 gas flow	10 l/min		1 l/min
Temperature	600℃		
Process time	3 hour		
Rotating rate	72 rpm	36 rpm	9 rpm

4. Result and Discussion

The observation results by SEM of the cross section of the test piece and the thickness of the deposited layer are shown in Table 3. The white lines in the SEM image shown in the upper part of the table indicate the nitrided layer and the deposited layer.From this table it is shown that deposited and nitrided layers are formed on the surface under all conditions. Condition 1 indicates that the deposited layer is the thinnest. Since the rotational speed of the furnace is the highest, it is considered that the deposited layer is less likely to be formed. However, the nitrided layer is considered to be thinner because the deposited layer is also a nitrogen source. Condition 2 indicates that the deposited layer and the nitrided layer are the thickest. As this factor, the large

flow rate of nitrogen gas and the influence of the rotational speed can be considered. Condition 3 had a value intermediate between Condition 1 and Condition 2 for both the nitride layer thickness and the deposited layer thickness. Although the flow rate of nitrogen gas is small, it is considered that the deposition rate is likely to be formed because the rotational speed is slow.From these results, it is understood that the aluminum alloy can be nitrided in a short time as compared with the conventional method. Furthermore, it can be seen that a deposited layer of abrasive is required to form a nitrided layer. In addition to this, it can be seen that the rotational speed of the furnace and the nitrogen gas flow rate greatly affect the formation of the nitrided layer and the deposited layer.

The measurement results of the hardness of the nitrided layer are shown in Fig.2. It can be seen from the figure that condition 3 shows the highest value. Also, it can be seen that there is a difference in the hardness of the nitrided layer depending on the conditions. Figure 3 shows the results of X-ray diffraction after removal of the deposited layer for the test piece under condition 1. From this result, it can be understood that the structure of the nitrided layer is AlN. Since similar results were shown under other conditions, it is necessary to consider factors that cause the hardness of the nitrided layer to differ.

Table 3 Result of SEM observation and Thickness of deposit layer

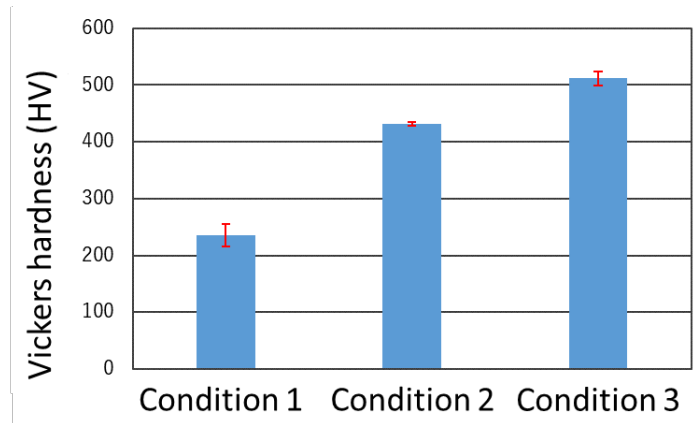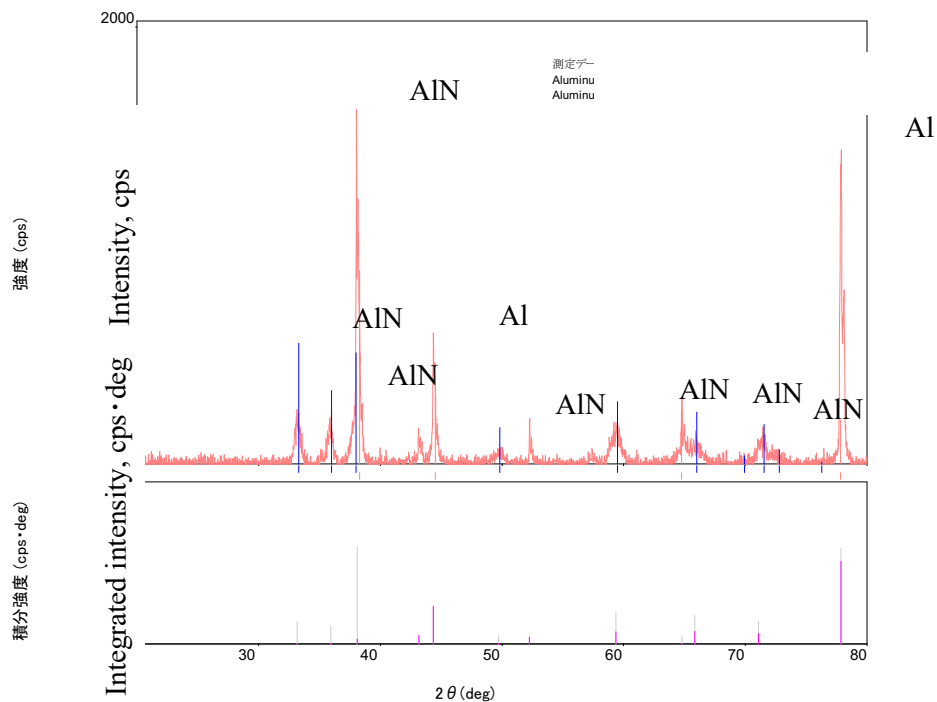|	Treatment condition 1	Treatment condition 2	Treatment condition 3
SEM observation			
Deposit layer Thickness (μm)	112	655	487

Fig. 2 Result of Hardness

Fig.3 Result of X-ray diffraction in condition 1

5. Conclusions

In this study, the influence of the treatment conditions on the formation of the diffusion layer in the barrel nitriding process was examined.

1. The deposit layer tended to increase with the increase of nitrogen flow rate. In addition, hardness also showed a tendency to increase
2. It was revealed that deposit and diffusion layers were formed in 3 hours or more of process time
3. In the selection of the optimum processing conditions, the deposited layer was thin, and the diffusion layer could obtain hardness of 500 HV or more.

References

1. M. Moradshahi, T. Tavakoli, S. Amiri, Sh. Shayeganmehr. Plasma nitriding of Al Alloys by DC discharge. Surface & Coating Technology, 2006, 567
2. J. Acosta, A. Rojo, O. Salas, J. Oseguera. Process monitoring during ALN deposition by reactive magnetron sputtering. Surface & Coating Technology, 2006, 7992
3. P. Vissutipitukul, T. Aizawa. Wear of plasma - nitrided aluminum alloys. Wear 2005, 482
4. M. Okumiya, H. Ikeda, Y. Tsunekawa. Study on nitriding mechanism for aluminum using barrel nitriding. Solid State Phenomena. 2006, 137-142.
5. M. Yoshida, M. Okumiya, R, Ichiki, W. Khalifa, C. Tekmen, Y. Tsunekawa, K. Tanaka. Mechanical properties of aluminum nitride layer formed by duplex coating of Barrel Nitriding and Plasma Nitriding. Plasma Process and Polymers. 2009, 310

Development and fabrication of graphene oxide membranes for water desalination

Kurbangali Tynyshtykbayev[1], Zarina Yelemessova [1], Zhaxylyk Yermogambetov[1], Zhanibek Balgin[1], Zinetula (Zeke) Insepov[1,2,3*]

[1]Nazarbayev University, Kabanbay batyr, 53, Nur Sultan, Republic of Kazakhstan
[2] National Nuclear Research University (MEPhI), Moscow, Russian Federation
[3] Purdue University, West-Lafayette, IN USA
* E-mail: zinsepov@purdue.edu

Abstract
In this work, the possibility of creating reduced graphene oxide/polyvynilidene fluoride (rGO/PVDF) membranes by using graphene oxide (GO) on the surface of standard polymeric PVDF membranes is shown. rGO/PVDF membranes have better filtration efficiency than standard polymer PVDF membranes. Increase in speed of transportation of water in rGO/PVDF membranes with the decrease in the sizes of nanochannels is experimentally shown. The feature of transportation of liquid via planar nanochannels of rGO membranes depending on rGO restoring time, which is explained by the decrease of activation energy of shear viscosity of the liquid in nanochannels.

Keywords: graphene oxide, reduced graphene oxide, membrane, PVDF, synthesis, nanochannels, filtration.

1. Introduction

rGO membranes with controlled nanoscale interlayer channels and pores are perspective for industrial desalination and water treatment thanks to economic technology of their creation and rich stocks of graphite. Their most attractive feature is the unique mechanism of water molecules transportation through nanoscale pores [1]. However, mechanisms of desalination and filtration of water through rGO membranes are not absolutely clear.
This work is devoted to the synthesis of composite rGO/PVDF membranes by using GO on a surface of polymeric PVDF membranes and to study the feature of water filtration depending on rGO reduction time.

2. Graphene oxide production technique

GO powders were prepared from graphite powder by the modified Hummers method [2]. To obtain reduced graphene oxide (rGO) the colloid GO suspension (3 mg of GO on 1 ml of H_2O) was treated in the ultrasonic bath for 3 hours. The resulting solution was mixed by mechanical stirrer at 80 °C for 12 hours. It led to the deposition of black powder of the rGO. After cooling to ambient temperature, rGO powder was sieved via filter with the subsequent reduction at 150 °C from 0.5 to 4 hours. For comparison GO of Sigma-Aldrich brand was used [3].

rGO/PVDF membranes prepared by a dispersion of the powders rGO in water with the subsequent ultrasonic influence within 30 min. Later GO was deposited on a polymeric PVDF membrane (Durapore Membrane Filter, 47 mm Hydrophilic PVDF membrane, pore size 0.22 μm) with vacuum filtration method (a two-stage vacuum pump of ROAIRVAC 1.5/3.0/6.0/9.0 R17300416 ROTHENBERGER, 500 Mbar) within 60 minutes at ambient temperature with subsequent drying at 40 ° C within 24 hours. For comparison, similar GO/PVDF membranes were also used.

3. Characterization of filters

The GO and rGO suspensions and rGO/PVDF membranes were characterized by Fourier Transformation Infrared Spectroscopy (FTIR) using NicoletiS10 FTIR. Surface morphology and structure of rGO membranes were investigated by Scanning Electron Microscope Fe SEM Auriga Crossbeam 540.

The filtration abilities of rGO/PVDF membranes were measured by using vacuum filtration pump (DA-15D, ULVAC KIKO, Inc.) with the pumping rate of 12 l/min and pressure of 6.65 kPa. pH of the solutions was measured by pH meter (HANNA HI 2550 pH/ORP & EC/TDS/NaCl Meter). Permeability tests was carried out by means of two-unit L-shaped compartments.

FTIR spectra of GO and rGO suspensions show the characteristic absorption bands of GO (Fig. 1).
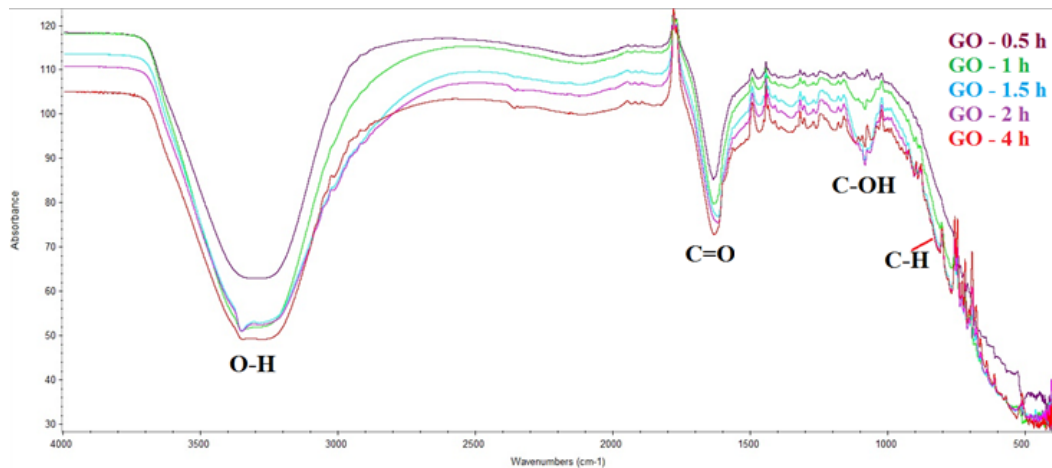

Figure 1 – FTIR absorption spectra of GO and rGO suspensions.

FTIR spectra show the characteristic absorption bands for OH - (3381 cm^{-1}, valent vibrations of OH – H bonds), CO- (1644 cm^{-1} valent vibrations of C = O– carbonyl group, deformation vibrations of H2O), C−OH- (1090 cm^{-1}, carboxyl group), CH - (870 cm^{-1}) [4]. With an increase GO reduction time, the amount of oxygen in hydroxyl OH and carboxyl CO- groups decreases, and the amount of hydrogen in them increases, which leads to the formation of predominantly hydrogen bonds between the functional groups on the surface of rGO sheets, which reduces the interlayer distance in them. The reduction process causes an increased dispersibility of the colloidal suspension of rGO and the aggregation of rGO– sheets by reducing oxygen and increasing hydrogen bonds with a predominant location of OH groups along the edges of the sheets [1]. That is, the absence or small amount of oxygen functional groups leads to a strong aggregation of rGO sheets, which leads to the formation of more defective rGO layers compared to GO layers.

In Fig, 2 SEM images of GO (a) and rGO (b) membranes are shown. It is clear that rGO membranes are more defective than GO membranes. The surface of rGO membranes and the edges of rGO sheets are uneven due to the aggregation of rGO. The surface and interlayered structure of the GO/PVDF membrane is homogeneous. The thickness of the GO layer consists of a larger number (15-20) of GO sheets and reaches 1500-1700 nanometers.

4. Filtration experiment

The experiment results of rGO/PVDF, GO/PVDF and PVDF membranes for filtering salt solution (pH 9.8) and filtration time (Table 1) showed that rGO/PVDF membranes are better than standard polymer PDVF membranes and GO/PVDF membranes.
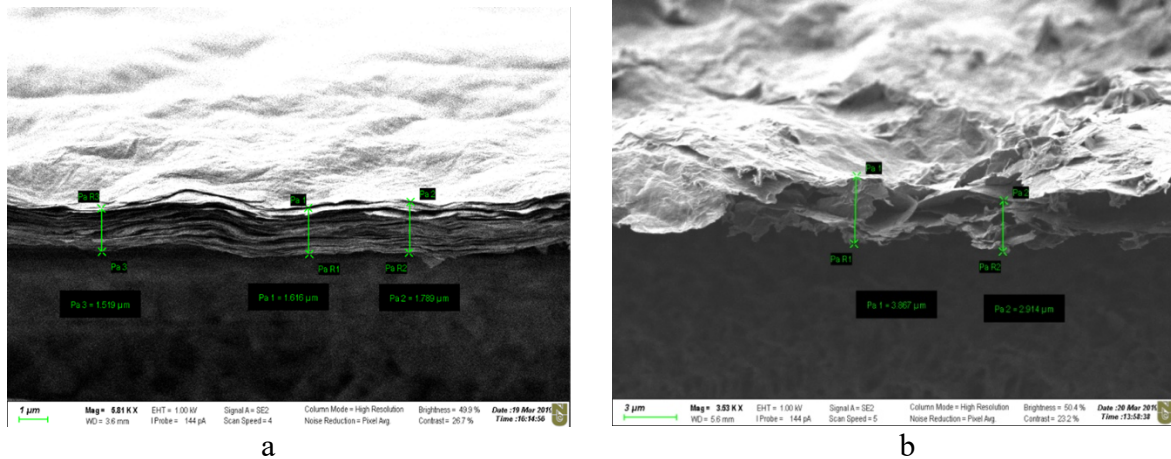
Figure 2 – SEM images GO (a) and rGO (b) membranes.

Table 1 – Filtration results of rGO/PVDF, GO/PVDF and PVDF membranes.

Membrane	pH	Filtration time, sec	
	Salt solution	Distilled water	Salt solution
PVDF	7.78	40	51
GO/ PVDF	7,56	23	28
rGO/PVDF (30 min)	7.02	80	134
rGO/ PVDF (60 min)	7.07	24	106
rGO/ PVDF (90 min)	7.09	24	31
rGO/PVDF (120 min)	7.63	17	25

The best results on filtration (pH-7.02) are shown by rGO/PVDF (30 min) membranes, on filtration time (25 sec) by rGO/PVDF (120 min) membrane.

In this work increase in the speed of transportation of water in composite rGO/PVDF membranes with a decrease in the sizes of nanochannels is experimentally shown. The most interesting results are received on the filtration time of rGO/PVDF, showing well permeability. As can be seen from the results of the experiment, table 1, at rGO/PVDF with an increase in reduction time decreases the time of passing of solutions through membranes. rGO membranes provide fast transportation of water in comparison with the membranes which not reduced GO membranes. Fluid flows through rGO (120 min) membranes more, than through rGO (60 min), and respectively through rGO (30 min) and GO membranes, i.e., the permeability of rGO (120 min) > rGO (60 min) > rGO (30 min) > GO membranes, respectively, that in inverse proportion to oxygen content in rGO membranes. Such behavior of transfer of water via planar nanochannels of the rGO membranes was observed [1] earlier. They showed an acceleration of water transportation through rGO membranes with a decrease in the sizes of planar nanochannels, the interlayered size between rGO layers. Authors of this work explain the acceleration of water transportation in planar graphene nanochannels of rGO membranes with the existence of not oxidized and reduced (hydrophobic) rGO areas which increase slip speed due to hydrophobicity and smoothness of these areas. Except for water hydrophobicity and smoothness of nanochannels, they use the theory of sliding flow [4] in carbon nanotubes (CNT) [5]. According to this theory acceleration of transport rate of water in CNT is possible because of the decrease of activation energy of shear viscosity of the liquid in nanoscale channels. According to the results of water molecules movement mechanisms in CNT [6], water flow rate increases with decrease CNT diameter that is caused by smaller surface interaction with water [7] and decrease of activation energy of shear viscosity of the liquid [8] which also depends on the diameter of the nanochannel [9].

5. Conclusion
Thus, we showed the possibility of creating efficient rGO/PVDF membranes by using GO on the surface in standard polymeric PVDF membranes. Composite rGO/PVDF membranes have the best effectiveness of

filtration than standard polymeric PVDF membranes. Increase in speed of water transportation in rGO/PVDF membranes with a decrease of the sizes of nanochannels is experimentally shown, that is explained by a decrease of activation energy of shear viscosity of the liquid in nanochannels.

Acknowledgements

References

1. H. Huanga, R. K. Joshib, K. Kanishk et.al. Fabrication of reduced graphene oxide membranes for water desalination. Journal of Membrane Science, 572, 12–19 (2019).
2. W.S.Hummers, R.E. Offeman. Preparation of Graphitic Oxide. J. Am. Chem. Soc, 80, 1339 (1958).
3. https://www.sigmaaldrich.com/catalog/product/aldrich/794341?lang=en&region=.
4. P. Bansal, A.S. Panwar, D. Bahadur. Molecular-level insights into the stability of Aqueous graphene oxide dispersions. J. Phys. Chem. ,121, 9847–9859 (2017).
5. Y. Han, Z. Xu, C. Gao. Ultrathin graphene nanofiltration membrane for water purification. Adv. Funct. Mater, 23, 3693–3700 (2013).
6. J.K. Holt, H.G. Park, Y. Wang, M. Stadermann, A.B. Artyukhin, C.P. Grigoropoulos, A. Noy, O. Bakajin. Fast mass transport through sub-2-nanometer carbon nanotubes. Science 312 (2006) 1034.
7. J.A. Thomas, A.J. McGaughey. Water flow in carbon nanotubes: transition to subcontinuum transport. Phys. Rev. Lett. 102, 184502 (2009).
8. S. Joseph, N. Aluru. Why are carbon nanotubes fast transporters of water? Nano Lett. 8, 452-458 (2008).
9. J.S. Babu, S.P. Sathian. The role of activation energy and reduced viscosity on the enhancement of water flow through carbon nanotubes. J. Chem. Phys., 134, 501-509 (2011).

Development and fabrication of graphene oxide membranes for water desalination

Kurbangali Tynyshtykbayev[1], Zarina Yelemessova [1], Zhaxylyk Yermogambetov[1], Zhanibek Balgin[1], Zinetula (Zeke) Insepov[1,2,3*]

[1]Nazarbayev University, Kabanbay batyr, 53, Nur Sultan, Republic of Kazakhstan
[2] National Nuclear Research University (MEPhI), Moscow, Russian Federation
[3] Purdue University, West-Lafayette, IN USA
* E-mail: zinsepov@purdue.edu

Abstract
In this work, the possibility of creating reduced graphene oxide/polyvynilidene fluoride (rGO/PVDF) membranes by using graphene oxide (GO) on the surface of standard polymeric PVDF membranes is shown. rGO/PVDF membranes have better filtration efficiency than standard polymer PVDF membranes. Increase in speed of transportation of water in rGO/PVDF membranes with the decrease in the sizes of nanochannels is experimentally shown. The feature of transportation of liquid via planar nanochannels of rGO membranes depending on rGO restoring time, which is explained by the decrease of activation energy of shear viscosity of the liquid in nanochannels.

Keywords: graphene oxide, reduced graphene oxide, membrane, PVDF, synthesis, nanochannels, filtration.

1. Introduction
rGO membranes with controlled nanoscale interlayer channels and pores are perspective for industrial desalination and water treatment thanks to economic technology of their creation and rich stocks of graphite. Their most attractive feature is the unique mechanism of water molecules transportation through nanoscale pores [1]. However, mechanisms of desalination and filtration of water through rGO membranes are not absolutely clear.
This work is devoted to the synthesis of composite rGO/PVDF membranes by using GO on a surface of polymeric PVDF membranes and to study the feature of water filtration depending on rGO reduction time.

2. Graphene oxide production technique
GO powders were prepared from graphite powder by the modified Hummers method [2]. To obtain reduced graphene oxide (rGO) the colloid GO suspension (3 mg of GO on 1 ml of H_2O) was treated in the ultrasonic bath for 3 hours. The resulting solution was mixed by mechanical stirrer at 80 °C for 12 hours. It led to the deposition of black powder of the rGO. After cooling to ambient temperature, rGO powder was sieved via filter with the subsequent reduction at 150 °C from 0.5 to 4 hours. For comparison GO of Sigma-Aldrich brand was used [3].
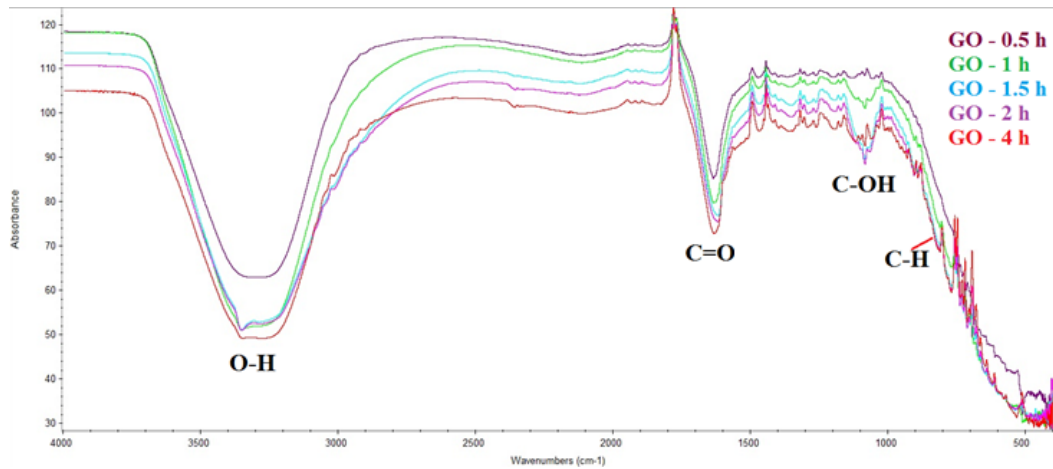
rGO/PVDF membranes prepared by a dispersion of the powders rGO in water with the subsequent ultrasonic influence within 30 min. Later GO was deposited on a polymeric PVDF membrane (Durapore Membrane Filter, 47 mm Hydrophilic PVDF membrane, pore size 0.22 μm) with vacuum filtration method (a two-stage vacuum pump of ROAIRVAC 1.5/3.0/6.0/9.0 R17300416 ROTHENBERGER, 500 Mbar) within 60 minutes at ambient temperature with subsequent drying at 40 ° C within 24 hours. For comparison, similar GO/PVDF membranes were also used.

3. Characterization of filters
The GO and rGO suspensions and rGO/PVDF membranes were characterized by Fourier Transformation Infrared Spectroscopy (FTIR) using NicoletiS10 FTIR. Surface morphology and structure of rGO membranes were investigated by Scanning Electron Microscope Fe SEM Auriga Crossbeam 540.
The filtration abilities of rGO/PVDF membranes were measured by using vacuum filtration pump (DA-15D, ULVAC KIKO, Inc.) with the pumping rate of 12 l/min and pressure of 6.65 kPa. pH of the solutions was

measured by pH meter (HANNA HI 2550 pH/ORP & EC/TDS/NaCl Meter). Permeability tests was carried out by means of two-unit L-shaped compartments.

FTIR spectra of GO and rGO suspensions show the characteristic absorption bands of GO (Fig. 1).
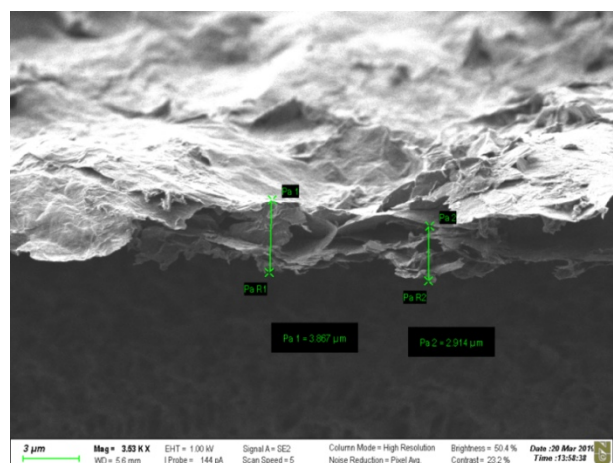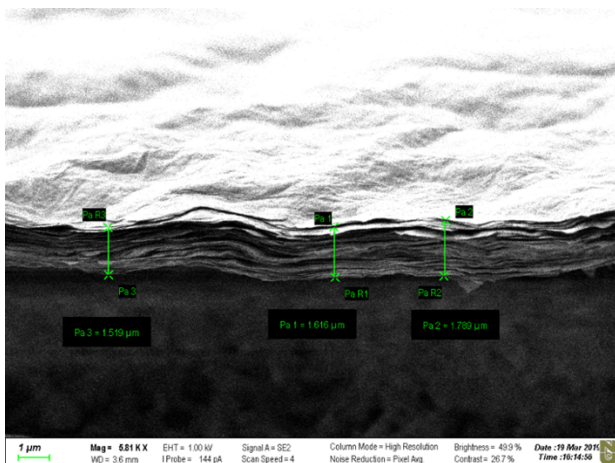

Figure 1 – FTIR absorption spectra of GO and rGO suspensions.

FTIR spectra show the characteristic absorption bands for OH - (3381 cm^{-1}, valent vibrations of OH – H bonds), CO- (1644 cm^{-1} valent vibrations of C = O– carbonyl group, deformation vibrations of H2O), C–OH- (1090 cm^{-1}, carboxyl group), CH - (870 cm^{-1}) [4]. With an increase GO reduction time, the amount of oxygen in hydroxyl OH and carboxyl CO- groups decreases, and the amount of hydrogen in them increases, which leads to the formation of predominantly hydrogen bonds between the functional groups on the surface of rGO sheets, which reduces the interlayer distance in them. The reduction process causes an increased dispersibility of the colloidal suspension of rGO and the aggregation of rGO– sheets by reducing oxygen and increasing hydrogen bonds with a predominant location of OH groups along the edges of the sheets [1]. That is, the absence or small amount of oxygen functional groups leads to a strong aggregation of rGO sheets, which leads to the formation of more defective rGO layers compared to GO layers.

In Fig, 2 SEM images of GO (a) and rGO (b) membranes are shown. It is clear that rGO membranes are more defective than GO membranes. The surface of rGO membranes and the edges of rGO sheets are uneven due to the aggregation of rGO. The surface and interlayered structure of the GO/PVDF membrane is homogeneous. The thickness of the GO layer consists of a larger number (15-20) of GO sheets and reaches 1500-1700 nanometers.

4. Filtration experiment

The experiment results of rGO/PVDF, GO/PVDF and PVDF membranes for filtering salt solution (pH 9.8) and filtration time (Table 1) showed that rGO/PVDF membranes are better than standard polymer PDVF membranes and GO/PVDF membranes.

A   B
Figure 2 – SEM images GO (a) and rGO (b) membranes.

Table 1 – Filtration results of rGO/PVDF, GO/PVDF and PVDF membranes.

Membrane	H	Filtration time, sec	
	Salt solution	istilled water	lt solution
VDF	7.78	40	51
O/ PVDF	7,56	23	28
GO/PVDF (30 min)	7.02	80	134
O/ PVDF (60 min)	7.07	24	106
O/ PVDF (90 min)	7.09	24	31
O/PVDF (120 min)	7.63	17	25

The best results on filtration (pH-7.02) are shown by rGO/PVDF (30 min) membranes, on filtration time (25 sec) by rGO/PVDF (120 min) membrane.

In this work increase in the speed of transportation of water in composite rGO/PVDF membranes with a decrease in the sizes of nanochannels is experimentally shown. The most interesting results are received on the filtration time of rGO/PVDF, showing well permeability. As can be seen from the results of the experiment, table 1, at rGO/PVDF with an increase in reduction time decreases the time of passing of solutions through membranes. rGO membranes provide fast transportation of water in comparison with the membranes which not reduced GO membranes. Fluid flows through rGO (120 min) membranes more, than through rGO (60 min), and respectively through rGO (30 min) and GO membranes, i.e., the permeability of rGO (120 min) > rGO (60 min) > rGO (30 min) > GO membranes, respectively, that in inverse proportion to oxygen content in rGO membranes. Such behavior of transfer of water via planar nanochannels of the rGO membranes was observed [1] earlier. They showed an acceleration of water transportation through rGO membranes with a decrease in the sizes of planar nanochannels, the interlayered size between rGO layers. Authors of this work explain the acceleration of water transportation in planar graphene nanochannels of rGO membranes with the existence of not oxidized and reduced (hydrophobic) rGO areas which increase slip speed due to hydrophobicity and smoothness of these areas. Except for water hydrophobicity and smoothness of nanochannels, they use the theory of sliding flow [4] in carbon nanotubes (CNT) [5]. According to this theory acceleration of transport rate of water in CNT is possible because of the decrease of activation energy of shear viscosity of the liquid in nanoscale channels. According to the results of water molecules movement mechanisms in CNT [6], water flow rate increases with decrease CNT diameter that is caused by smaller surface interaction with water [7] and decrease of activation energy of shear viscosity of the liquid [8] which also depends on the diameter of the nanochannel [9].

5. Conclusion
Thus, we showed the possibility of creating efficient rGO/PVDF membranes by using GO on the surface in standard polymeric PVDF membranes. Composite rGO/PVDF membranes have the best effectiveness of filtration than standard polymeric PVDF membranes. Increase in speed of water transportation in rGO/PVDF membranes with a decrease of the sizes of nanochannels is experimentally shown, that is explained by a decrease of activation energy of shear viscosity of the liquid in nanochannels.

Acknowledgements

References
1. H. Huanga, R. K. Joshib, K. Kanishk et.al. Fabrication of reduced graphene oxide membranes for water desalination. Journal of Membrane Science, 572, 12–19 (2019).

2. W.S.Hummers, R.E. Offeman. Preparation of Graphitic Oxide. J. Am. Chem. Soc, 80, 1339 (1958).
3. https://www.sigmaaldrich.com/catalog/product/aldrich/794341?lang=en&region=.
4. P. Bansal, A.S. Panwar, D. Bahadur. Molecular-level insights into the stability of Aqueous graphene oxide dispersions. J. Phys. Chem. ,121, 9847–9859 (2017).
5. Y. Han, Z. Xu, C. Gao. Ultrathin graphene nanofiltration membrane for water purification. Adv. Funct. Mater, 23, 3693–3700 (2013).
6. J.K. Holt, H.G. Park, Y. Wang, M. Stadermann, A.B. Artyukhin, C.P. Grigoropoulos, A. Noy, O. Bakajin. Fast mass transport through sub-2-nanometer carbon nanotubes. Science 312 (2006) 1034.
7. J.A. Thomas, A.J. McGaughey. Water flow in carbon nanotubes: transition to subcontinuum transport. Phys. Rev. Lett. 102, 184502 (2009).
8. S. Joseph, N. Aluru. Why are carbon nanotubes fast transporters of water? Nano Lett. 8, 452-458 (2008).
9. J.S. Babu, S.P. Sathian. The role of activation energy and reduced viscosity on the enhancement of water flow through carbon nanotubes. J. Chem. Phys., 134, 501-509 (2011).